THE JOURNAL OF PHYSICAL CHEMISTRY C
A JOURNAL OF THE AMERICAN CHEMICAL SOCIETY

pubs.acs.org/JPCC

Article

Spatial Separation of Enantiomers by Field-Modulated Surface Scattering

Yun Chen, Long Xu, Michael Urbakh, and Oded Hod*

Cite This: J. Phys. Chem. C 2023, 127, 10997−11004

Read Online

ACCESS | Metrics & More | Article Recommendations | Supporting Information

ABSTRACT: A new optomechanical chiral resolution scheme for molecules possessing a permanent dipole moment is proposed. The approach involves the following molecular manipulation sequence: (i) a molecular alignment electromagnetic pulse, (ii) a time-delayed dipole orienting static electric field, and (iii) scattering from a frictional surface. The method offers various control parameters including pulse duration and intensity, static field strength, delay time, surface dynamic friction coefficient, and incident molecular velocity that can be tuned to optimize spatial enantioseparation. The scheme is demonstrated for the prototypical HSOH chiral molecule, predicting an enantiomeric excess as high as 50%.

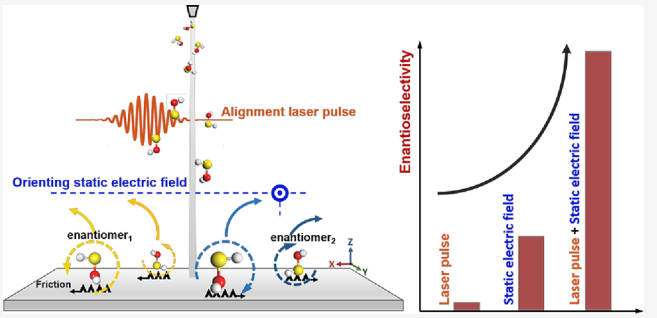

INTRODUCTION

Chirality is a geometrical asymmetry property, where the two mirror images of a given object do not superimpose and are hence distinguishable. As early realized by Louis Pasteur,[1] molecular chirality is of fundamental importance in chemistry and biology and may hold the key to deciphering the conundrum of life's origin, as well as play a central role in space exploration after extraterrestrial life.[2,3] Due to the predominance of homochirality in nature, homochiral synthesis and enantioseparation of racemic mixtures have raised broad interest in many fields associated with biochemistry and medicine.[4−12]

Because of the practical limitations of homochiral synthesis,[10] most research has been invested in developing viable methods for efficient enantioseparation. To date, the leading enantioseparation techniques, which demonstrate the highest performance, are chromatography-based.[8,13−16] These technologies, however, confront several obstacles, the most critical of which is the lack of a universal selector. This, in turn, necessitates the use of chiral resolution media tailored to each target molecule, which involves extensive and expensive research and development stages and limits the general applicability of the technology. To remedy the aforementioned deficiencies, a variety of new innovative technologies have emerged in recent years, including the usage of enantioselective membranes,[6,15,17] nanoparticles and nanomaterials,[10,18] ionic liquids,[10] and magnetized substrates,[19] as well as chiroptical methods.[20−29] Optical means have also been utilized to obtain spatial control over chiral molecules.[30−42] In this respect, techniques for realizing efficient molecular alignment are relatively well-established, often using a linearly polarized laser pulse to direct the most polarizable molecular principal axis of inertia along the polarization direction of the field.[31−34] Furthermore, strong uniform static electric fields were shown to induce molecular orientation (namely, unidirectional alignment) of simple molecules possessing a permanent dipole moment.[43−45] It was also demonstrated that optical stereodynamic control can be a powerful tool for modifying molecule−surface scattering and molecule−surface reactions.[46−52] Particularly, laser-controlled molecular surface scattering has been suggested for the separation of molecular isotopes and nuclear spin isomers.[51,52]

Another promising enantioseparation approach that is based on the generic characteristics of chiral objects and has the potential to provide universal selectivity is mechanical chiral resolution. This field of research aims to harness the asymmetric coupling of hydrodynamic interactions, shear forces, electric fields, and electromagnetic waves with chiral objects as a tool for distinguishing and resolving different enantiomers.[11,53] The realizations of this approach include the propeller effect found in chiral colloidal mixtures and chiral molecules;[54,55] De Gennes' suggestion of chiral microcrystal separation when pushed by a uniform force across a liquid surface;[56] rheological chiral separation utilizing nonuniform flow fields that exert different forces on molecules of opposite handedness;[11] resolution in microfluidic devices producing

Received: January 22, 2023
Revised: May 3, 2023
Published: June 6, 2023

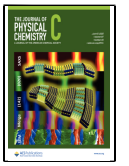

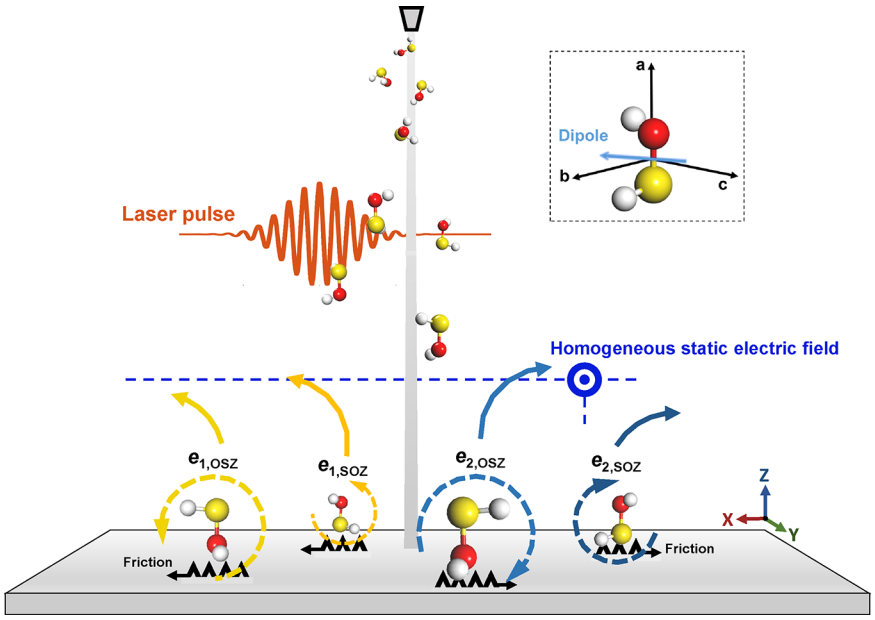

Figure 1. Schematic illustration of the enantioseparation scheme. From top to bottom, the initial uniform beam of randomly oriented molecules passes through a laser pulse that induces molecular alignment followed by a homogeneous electrostatic field that induces dipole orientation. Here, $e_{i,\,SOZ(OSZ)}$ marks the orientation of enantiomer i = 1,2 with the S−O (O−S) bond aligned with the Z axis. Collision with the surface results in opposite torque experienced by the two enantiomers, leading to opposite rotational senses and inverse friction forces acting in the lateral x direction. This, in turn, results in opposite scattering azimuthal directions and spatial enantioseparation. The inset shows the principal axes of inertia and the permanent dipole moment of the molecule. Red, yellow, and gray spheres represent oxygen, sulfur, and hydrogen atoms, respectively.

nonuniform laminar flows, helical flow fields, and vortices;[11,57−64] and the chiral vortex effect in gas flows generated by molecular drag pumps.[65−68] While their quantitative efficiency for enantioseparation varies depending on the specific chemical composition or geometric arrangement of the target moieties, common to all these methods is the fact that their qualitative nature relies on the general chiral asymmetry of the objects and is hence universal. Mechanical chiral resolution, therefore, emerges as a promising robust approach for enantioseparation of chiral objects at various scales ranging from the molecular level to the nano- and microscales.

In the present paper, we propose a novel scheme that combines optical manipulation and mechanical chiral resolution for the spatial separation of enantiomers possessing a finite permanent dipole moment and anisotropic polarizability. The scheme is based on the following consecutive steps: first, selective gas-phase preorientation of different enantiomers in mirror symmetric configurations is achieved using a linearly polarized laser pulse followed by a strong homogeneous static electric field; then spatial enantio-selectivity is achieved by scattering the preoriented enantiomers from a frictional surface. Each component in this scheme plays a predefined role: the pulse prealigns the chiral molecules with respect to the surface, the static field then orients the aligned enantiomers in mirror image configurations, surface collision of the oriented enantiomers results in opposite-sense molecular rotations, and surface friction induces scattering of the two enantiomers in different spatial directions.

To demonstrate the approach, we consider the prototypical hydrogen thioperoxide (HSOH) chiral molecule, the structural and chemical simplicity of which allows for a clear interpretation of the computational results, as previously demonstrated in the context of enantiomeric differentiation.[31−33] While the racemization barrier of this molecule is quite low,[31,69,70] we do not observe any collision-induced racemization events throughout our simulations. The three principal axes of inertia of the molecule are presented in Figure 1, where the most polarizable direction is along the S−O bond, marked as the a principal axis of inertia. The application of a femtosecond pulse propagating in the XY plane and polarized along the vertical (Z) direction in the laboratory frame (see Figure 1), therefore, aligns the S−O bond of the molecules along the Z axis with either the oxygen (red) or sulfur (yellow) atoms pointing toward the surface. The permanent dipole moment of the molecule (marked by the blue arrow in the inset of Figure 1) points almost perpendicular to the S−O bond and toward the bisector of the molecular dihedral angle.[31] By applying a static electric field in the Y direction, parallel to the surface, the molecules rotate around the S−O bond to orient their dipole moment with the field. As a result, opposite enantiomers assume mirror image configurations with respect to the plane formed by the dipole moment and the a principal axis of inertia (namely, the YZ plane in the laboratory frame) as shown at the bottom of Figure 1. Therefore, when approaching the surface, the O−H or S−H bonds of opposite enantiomers hit it in mirror image orientations. The resulting torque, acting mainly in the Y direction, has an opposite sign for the two enantiomers, inducing rotation in opposite senses. Hence, the surface friction force acts on the two enantiomers in inverse lateral directions, resulting in opposite scattering angles and eventual spatial enantioseparation.

METHODS

An explicit demonstration of this mechanism can be achieved by performing fully atomistic molecular dynamics simulations. We find that with an appropriate choice of Hamiltonian and parameterization of the light−molecule interactions, classical

https://doi.org/10.1021/acs.jpcc.3c00502
J. Phys. Chem. C 2023, 127, 10997−11004

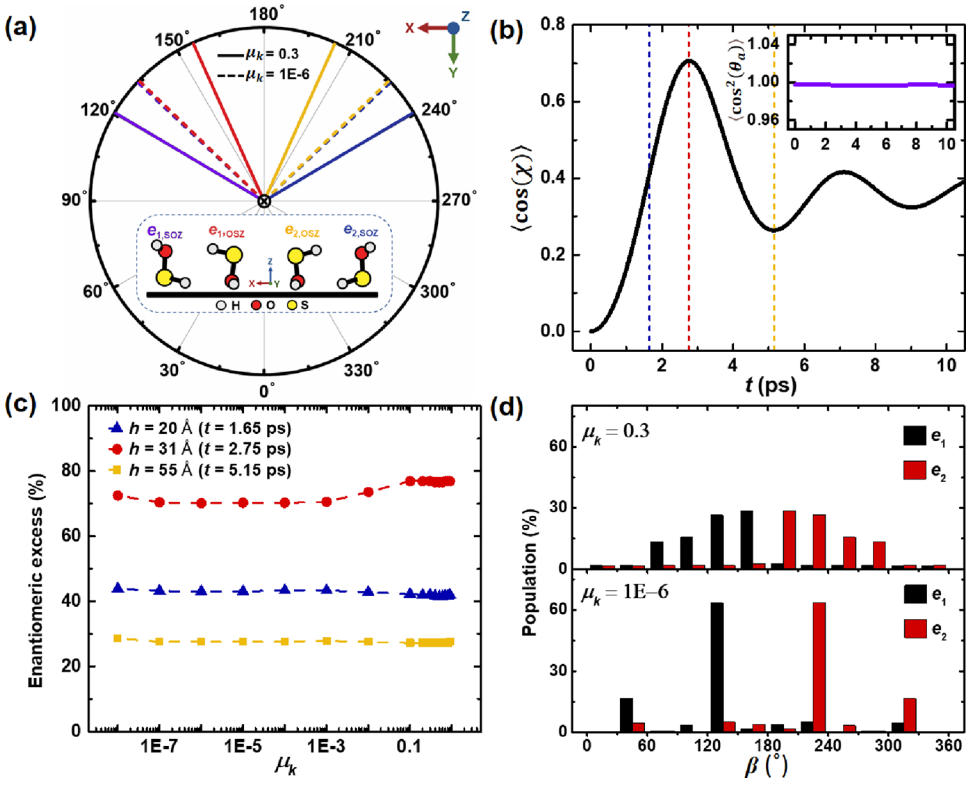

Figure 2. (a) Azimuthal scattering angle, β, of the two rigid HSOH enantiomers, prealigned along the vertical axis in two different orientations illustrated by the corresponding ball-and-stick models. Purple and red (blue and yellow) lines correspond to the two orientations of enantiomer 1 (2). Two surface friction coefficients are considered: $\mu_k = 10^{-6}$ (dashed lines) and $\mu_k = 0.3$ (solid lines). (b) Dynamics of the degree of dipole orientation given by the average of the cosine azimuthal angle, $\langle\cos(\chi)\rangle$, for an ensemble of 720 vertically aligned rigid e_1 enantiomers, under a static electric field of 50 kV/cm applied in the Y direction (see Figure 1). Here, an initial uniform distribution of the azimuthal angle of the permanent molecular dipole moment is considered. The inset shows the time dependence of the degree of alignment, $\langle\cos^2(\theta_a)\rangle$. (c) Friction dependence of the enantiomeric excesses of the scattered molecular ensemble with three different initial heights, resulting in different average dipole orientations at the moment of impact with the surface. The colors correspond to the vertical dashed lines appearing in panel (b) indicating the corresponding ensemble average dipole orientation at the moment of impact. (d) Angular distribution of the scattered molecular ensembles of the two HSOH enantiomers colliding with surfaces of dynamic friction coefficients $\mu_k = 10^{-6}$ and 0.3. Results are shown for an initial height of 31 Å, corresponding to maximal ensemble averaged dipole orientation at the point of impact, marked by the vertical dashed red line in panel (b).

molecular dynamics provides a reliable representation of the system considered (see Supporting Information (SI) Section S1). Hence, we developed a classical simulation scheme, implemented within the LAMMPS software,[71] that includes the following procedures: (i) intramolecular interactions are described via the OPLS-AA force field;[72] (ii) light−molecule interactions are described via the permanent dipole vector and polarizability tensor (see SI Section S1.1), which have been precalculated using density functional theory at the level of CAM-B3LYP/aug-cc-pVTZ,[73] as implemented in the Gaussian 16 package;[74] (iii) to treat the molecule−surface scattering, we adopt a rigid wall model and describe the molecule−surface interactions using the 9-3 Lennard-Jones (LJ) potential,[75] which mimics the interaction with a laterally infinite and vertically semi-infinite polarizable surface. This represents surfaces that are atomically smooth at the molecular scale, such that upon impact, the molecule does not experience random scattering due to surface roughness or contaminants. Furthermore, our surface model neglects nondispersive surface reactivity effects that may cause covalent molecular trapping. In practice, surfaces of layered material, such as graphene or graphite that are often used in nonreactive scattering research, may serve for this purpose.[76−79] Therefore, we use LJ parameters adapted for graphene (see SI Section S1.2).[80] Finally, the lateral dynamic friction force acting on atom i due to the rigid surface is described via an Amonton-type term of the form $f_i = -\mu_k|N_i|v_i^{\parallel}/|v_i^{\parallel}|$, where μ_k is the dynamic friction coefficient, $|N_i|$ is the magnitude of the normal force experienced by atom i due to the LJ interaction, and $v_i^{\parallel}/|v_i^{\parallel}|$ is a unit vector pointing along the direction of the lateral velocity of the atom. We note that the friction term is applied only in regions where the normal force, N_i, is repulsive, namely, pointing upward and away from the surface. In the present study, all simulations are performed at zero temperature ($T = 0$ K) while neglecting intermolecular interactions. More details regarding the computational approach are provided in SI Section S1.

RESULTS AND DISCUSSION

First, to demonstrate that indeed perfectly oriented enantiomers scatter in different directions, we use the developed tool to perform surface scattering simulations of the two rigid HSOH enantiomers, the center-of-masses of which are positioned 2 nm above the surface and are given an initial normal velocity of 1,000 m/s toward the surface. The initial alignment of the molecules in these calculations is depicted in the inset of Figure 2a. The main panel in Figure 2a shows the lateral projection of the molecular center-of-mass velocity vector after 8 ps, where the vertical distance of the scattered

https://doi.org/10.1021/acs.jpcc.3c00502
J. Phys. Chem. C 2023, 127, 10997−11004

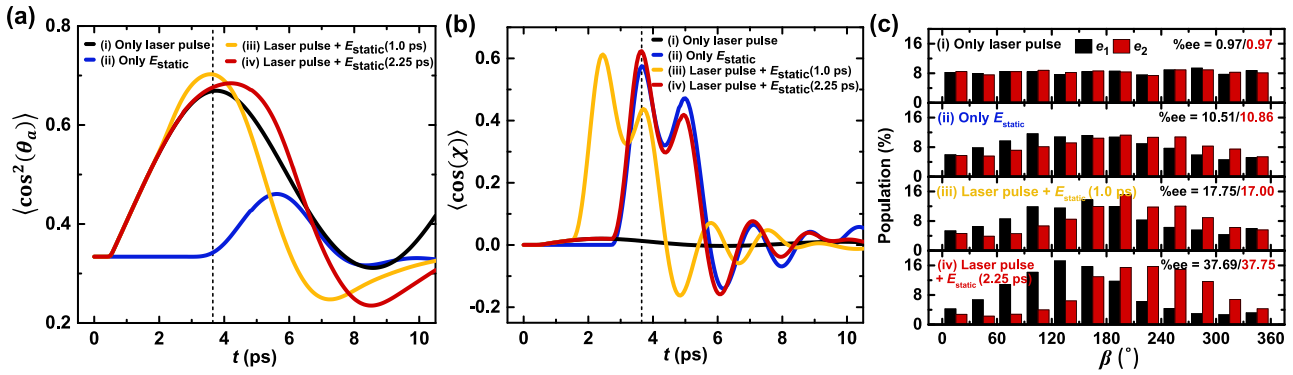

Figure 3. Enantioselectivity for different manipulation protocols, including (i) only the vertical alignment laser pulse (black), (ii) only the lateral orienting static electric field at time t = 2.75 ps (blue), (iii) a laser pulse followed by a static electric field with a delay of 1 ps (yellow), and (iv) a laser pulse followed by an electric field with a delay of 2.25 ps (red). (a) Time dependence of the S−O bond vertical alignment factor $\langle\cos^2(\theta_a)\rangle(t)$ for an ensemble of N = 18,000 HSOH rigid molecules, whose initial orientations are randomly chosen from a uniform distribution. (b) Time dependence of the dipole lateral orientation factor $\langle\cos(\chi)\rangle(t)$ with respect to the static field direction, for the same molecular ensemble. (c) Angular scattering distributions obtained using the four manipulation protocols for the two enantiomers (black and red columns) with a vertical incident velocity of 1,000 m/s following scattering at t = 3.7 ps (dashed lines in panels (a) and (b)) from a surface of dynamic friction coefficient of μ_k = 0.3. The two values provided for the enantiomeric excess are calculated for the two spatial regions β = 0 − 180° (e_1) and β = 180 − 360° (e_2). The minor differences found between them result from the finite size of the simulated molecular ensemble.

molecules from the surface exceeds 2 nm. For each enantiomer, we consider the two possible alignments and several friction coefficients. In the absence of friction (μ_k = 0), the molecules are reflected up in the normal direction, leaving no projection traces along the lateral dimensions, thus demonstrating no spatial enantioselective scattering. When switching on a very small friction coefficient of $\mu_k = 10^{-6}$, preoriented opposite enantiomers scatter in mirror image directions with trajectories that only slightly deviate from the vertical axis. Notably, the projection of these trajectories on the lateral plane features a substantial angular separation of 90°. Increasing the friction coefficient to μ_k = 0.3 provides larger trajectory deviations from the vertical axis with not only spatial enantioseparation but also discrimination between the two possible alignments of each preoriented enantiomer. This is attributed to the enhanced effect of friction on the molecular conformation during impact, which is manifested differently at the two orientations, with either O or S atoms approaching the surface.

These simulations demonstrate enantioselective scattering of individual molecules with specific prechosen initial configurations, where the initial alignment of the S−O bond along the vertical axis mimics the effect of the laser pulse and the orientation of the dipole moment mimics the effect of the static uniform electric field. To demonstrate the dynamic effect of the latter, we extend our calculations to an ensemble of 1,440 rigid HSOH molecules (with no intermolecular interactions) under a static uniform electric field of E_Y = 50 kV/cm. The initial alignment of the S−O bond of all molecules is kept along the vertical axis, while an initial uniform distribution of the azimuthal angle of the permanent molecular dipole moment with respect to the field direction is considered, with an angular grid step of 1°. To this end, for each vertical orientation of the S−O bond of the two enantiomers (see illustration in Figure 2a), 360 scattering simulations are performed for any given initial height above the surface. Figure 2b presents the dynamics of the orientational degree of freedom, characterized by the ensemble averaged cosine of the azimuthal dipole moment angle, $\langle\cos(\chi)\rangle$. Upon the application of a constant field in the Y direction, all dipoles rotate toward the field direction, resulting in an initial increase in $\langle\cos(\chi)\rangle$. In the absence of a dissipative mechanism, this is followed by periodic oscillations of each dipole around the direction of the field. Notably, since we consider the entire range of azimuthal angles (not only small with respect to the field direction), the dynamics is generally anharmonic, and the oscillation periods of dipoles starting at different initial angles are not the same. Hence, the value of the first peak of $\langle\cos(\chi)\rangle$ is smaller than one, and the amplitude of the averaged angle oscillations decays with time to a value that is dictated by the span of periodicities of the different dipole oscillations (see SI Section S2.1). The inset of panel (b) shows the temporal evolution of the degree of alignment, $\langle\cos^2(\theta_a)\rangle$, where the polar angle, θ_a, is defined as the angle between the S−O axis of the molecule and the axis normal to the scattering surface. As expected, the curve demonstrates minor fluctuations near the value of $\langle\cos^2(\theta_a)\rangle$ = 1, indicating that the uniform electric field has a minor effect on the molecular alignment in this case.

This ensemble dipole orientation dynamics can be utilized for surface scattering-induced enantioseparation. Naturally, the enantioselectivity efficiency depends on the distribution of molecular orientations at the moment of impact with the scattering surface and on the friction coefficient. Figure 2c shows the enantiomeric excess as a function of the friction coefficient for three different molecular orientation distributions obtained at different times, marked by the three vertical dashed lines in Figure 2b. Here, the enantiomeric excess is defined as $100 \times |N(e_1) - N(e_2)|/[N(e_1) + N(e_2)]$, where $N(e_{1/2})$ is the number of $e_{1/2}$ enantiomers scattered in the positive (or negative) x axis direction. The three curves are obtained by providing all molecules with the same initial normal center-of-mass velocity of 1,000 m/s toward the surface while positioning them at different initial heights above the surface (20, 31, and 55 Å) so that the impact times correspond to 1.65, 2.75, and 5.15 ps (depicted, as well, by the vertical dashed lines in Figure 2b). Naturally, for a frictionless surface, no enantiomeric excess is obtained. Once friction is turned on, an enantiomeric excess as high as 75% is obtained when the degree of ensemble averaged dipole orientation in the lateral plane is maximal at the moment of impact. Notably, the

https://doi.org/10.1021/acs.jpcc.3c00502
J. Phys. Chem. C 2023, 127, 10997−11004

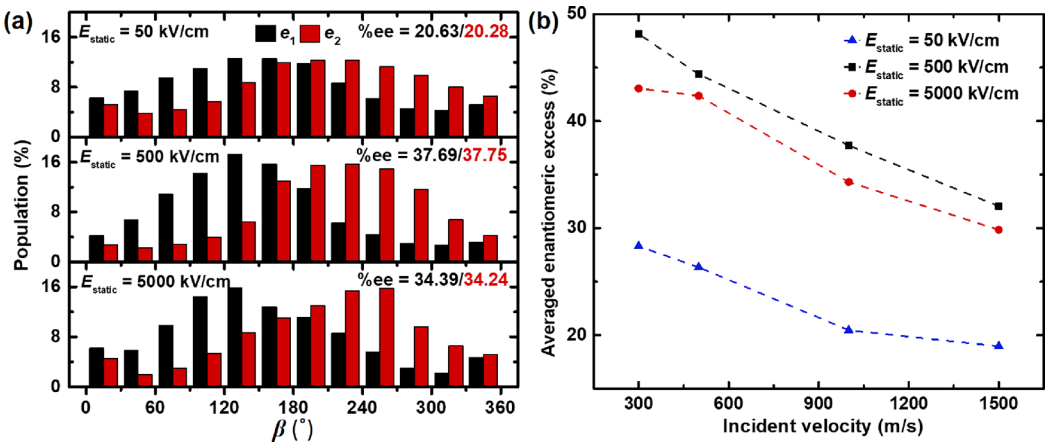

Figure 4. Effect of static field strength and vertical incident velocity on enantioselectivity for an ensemble of N = 18,000 HSOH rigid molecules, whose initial orientations are randomly chosen from a uniform distribution. (a) Angular distributions of the two enantiomers (black and red columns) with an initial vertical velocity of 1,000 m/s for static field strengths of 50, 500, and 5,000 kV/cm at time delays of 0.8, 2.25, and 2.9 ps from the maximal pulse intensity, respectively. (b) Velocity dependent enantiomeric excesses at static field strengths of 50, 500, and 5,000 kV/cm. In these cases, scattering from a surface of dynamic friction coefficient of μ_k = 0.3 occurs at t = ∼ 3.7 ps.

scattering azimuthal angle is found to be practically independent of the value of the dynamic friction coefficient down to $\mu_k = 10^{-8}$, whereas the corresponding altitude angle exhibits linear dependence on the friction coefficient in the range $\mu_k = 10^{-8} - 0.01$ (see SI Section S2.2). This leads to weak dependence of the overall enantiomeric excess on the dynamic friction coefficient. Figure 2d presents the distribution of azimuthal scattering angles, β (defined as the angle between the lateral projection of the molecular center-of-mass velocity vector and the Y axis), for two values of the dynamic friction coefficient: $\mu_k = 10^{-6}$ and 0.3. Once friction is turned on, we find well-separated scattering angle distributions for the two enantiomers peaking at angles that correspond to those presented in Figure 2a for the preoriented molecules.

The above analysis demonstrates the role of the azimuthal molecular dipole orientation distribution upon impact with a frictional surface on the spatial enantioselective scattering of chiral molecules. The final matter that remains to be investigated is the effect of prealignment of the S−O molecular axis along the surface normal. This can be achieved via a Gaussian electromagnetic pulse of the form $\boldsymbol{E}(t) = E_0\, e^{-2\ln(2)(t-t_0)^2/\sigma^2}\cos(\omega t)\hat{\boldsymbol{z}}$ polarized along the vertical direction ($\hat{\boldsymbol{z}} = (0,0,1)$), where E_0 is the peak amplitude of the laser pulse, σ is its full-width at half-maximum (FWHM), ω is the carrier frequency, and t_0 is the pulse center.[81] Since the carrier frequency is larger than the typical molecular rotation frequency by several orders of magnitude, we may average the pulse intensity ($|\boldsymbol{E}(t)|^2$) over the rapid optical cycle.[82] Furthermore, if $\sigma \gg 2\pi/\omega$, we can take the Gaussian envelope out of the integration, allowing us to approximate the pulse by its envelope $|\mathbf{E}(t)|^2 \approx \frac{1}{2}E_0^2\, e^{-4\ln(2)(t-t_0)^2/\sigma^2}$.

We consider an ensemble of 18,000 (9,000 for each enantiomer) uniformly distributed and randomly oriented noninteracting rigid HSOH molecules. The vertical Gaussian pulse (σ = 0.1 ps, E_0 = 84.85 MV/cm, t_0 = 0.5 ps) is applied at the beginning of the simulation (t = 0 ps), and a static field of 500 kV/cm is switched on in the Y direction with delays of 1.0 and 2.25 ps from the maximal pulse intensity. Figure 3a,b presents the time evolution of the vertical alignment of the S−O molecular axis and the lateral dipole orientation, for the two delays considered in the absence of a scattering surface. For both delays (yellow and red curves), maximal vertical alignment is obtained at 3 − 3.7 ps following the peak pulse intensity (see Figure 3a). Notably, for a time delay of 2.25 ps between the pulse and the static field, maximal lateral dipole orientation is obtained nearly simultaneously with the peak vertical S−O bond alignment (see dashed black lines in Figure 3a,b). For a time delay of 1.0 ps, the maximal vertical S−O bond alignment lags by 1.25 ps behind the lateral dipole moment orientation. It is only the secondary peak of the latter that matches the main peak of the former. Based on the above analysis, a time delay of 2.25 ps is expected to provide optimal conditions for achieving efficient enantioselectivity upon impact with the frictional surface.

Figure 3c shows the angular enantiomer scattering distributions obtained when applying the following protocols: (i) only the vertical alignment laser pulse (top panel), (ii) only the lateral orienting electric field (second panel from top), (iii) a laser pulse followed by an electric field with a delay of 1 ps (second panel from bottom), and (iv) a laser pulse followed by an electric field with a delay of 2.25 ps (bottom panel). In these simulations, the scattering occurs from a surface of dynamic friction coefficient of μ_k = 0.3 at a time t = 3.7 ps (see black dashed vertical lines in Figure 3a,b). For the first protocol (only alignment pulse application), a nearly uniform angular distribution is obtained with very low enantiomeric excess (∼1% with the ensemble size used herein). Applying only the static electric field reduces the angular distribution uniformity, leading to an increase of enantiomeric excess to ∼11%. The combined application of the alignment pulse and orientation field with a time delay of 1.0 ps further increases the enantioselectivity to an excess of ∼17%. Notably, at the optimal time delay, an angular separation of the peak distribution for the two enantiomers is clearly seen with a significant enantiomeric excess approaching 40%. This signifies that the delay between the alignment pulse and the application of the orienting static electric field is an important parameter for achieving optimal enantioselectivity.

By comparing the two upper panels of Figure 3c, it is evident that the molecular dipole orientation due to the static electric field is central for obtaining efficient enantioselectivity.

https://doi.org/10.1021/acs.jpcc.3c00502
J. Phys. Chem. C 2023, 127, 10997−11004

Therefore, to further investigate the effect of field strength on the separation efficiency, we repeat our simulations for various field intensities. Figure 4a presents the scattering angular distributions of the two enantiomers for static field strengths of 50, 500, and 5,000 kV/cm at time delays of 0.8, 2.25, and 2.9 ps, where maximal enantioselectivity is achieved. We find that reducing the field to 50 kV/cm reduces the enantiomeric excess from ∼38 to ∼20%. This is attributed to the fact that at weaker fields, maximal lateral orientation is not achieved. At the strongest field considered (5,000 kV/cm), the maximal orientation achieved is similar to that obtained for 500 kV/cm. Nonetheless, a smaller enantiomeric excess of ∼34% is obtained. This is attributed to the fact that under the stronger field, the molecular ensemble accumulates higher angular momentum and hence loses orientation faster during collision while within the interaction range with the scattering surface (see SI Section S2.3 for further details).

Another important parameter for optimizing the enantioselectivity of the proposed approach is the vertical incident velocity of the molecules with the scattering frictional surface. To evaluate the velocity effect, we repeated the scattering calculations with different initial vertical velocities. To isolate the effect of velocity, we assure that in these simulations, all molecules spend the same time under the action of the external fields, by adjusting their initial height according to their vertical velocity. Figure 4b presents the dependence of the enantiomeric excess on the initial vertical velocity for several static electric field strengths, showing enantiomeric excess as high as ∼50% at the lower velocities considered with a general decrease with increasing velocity. As discussed in SI Section S2.4, this results from transfer of translational to rotational energy upon collision with the surface.[83] Given a higher initial center-of-mass velocity, the molecule accumulates higher angular momentum during collision, which results in faster deviation of the ensemble distribution from the optimal dipole orientation and reduced enantioselectivity. We note that at velocities sufficiently lower than ∼300 m/s, the molecules remain trapped at the surface, and the simulation results become irrelevant for enantioseparation modeling.

CONCLUSIONS

We therefore see that under appropriate conditions, the proposed approach for spatial enantioseparation of a molecular beam, based on a combination of optical manipulation and dissipative surface scattering, is predicted to achieve significant enantiomeric excess for molecules possessing a permanent dipole moment. This requires the following manipulation sequence: (i) a molecular alignment electromagnetic pulse, (ii) a time-delayed dipole orientation static electric field, and (iii) scattering from a frictional surface. While we consider classical simulations of rigid molecular models performed at zero temperature, test calculations indicate that quantum mechanical effects have a minor contribution to the molecular preorientation at the scattering timescale considered (see SI Section S2.5), and that including molecular flexibility yields the same qualitative enantioselectivity trends with a small quantitative effect (see SI Section S2.6). Furthermore, while thermal effects may influence molecular alignment and hence reduce enantioseparation efficiency (see SI Section S2.7), increasing the alignment field intensity may offer a remedy for this problem. Importantly, under optimal conditions, the proposed mechanism is expected to realize highly efficient enantiomeric separation, which is comparable to other optical enantioseparation schemes.[22,25,26] The method offers various control parameters including pulse duration and intensity, static field strength, delay time, surface friction coefficient, and initial molecular velocity that can be tuned to optimize the spatial enantioseparation of the molecule of interest. Notably, the method is not limited to the HSOH test case discussed and is applicable to a wide family of polar molecules, as demonstrated in SI Section S3. We further note that while we present a proof-of-concept study of a new field-manipulated molecular frictional enantioseparation mechanism, present experimental capabilities are currently unable to obtain the high-precision field focusing required to achieve maximal enantioseparation efficiency. Nonetheless, even with present capabilities, enantioseparation efficiencies as high as 10% can be obtained in the presence of the static field alone without the need for pulse focusing (see Figure 3c) and as high as 20% when applying the laser pulse simultaneously with the static field, thus eliminating the delay time altogether (see SI Section S2.9). With the natural development of measurement technology, the potential of the proposed approach is expected to be fully exploited. Finally, we note that terahertz (THz) and two-color laser pulses have been recently predicted to facilitate dipole orientation of chiral molecules,[37,39,40] which suggests that they can replace the uniform electrostatic field in our approach resulting in an all-optical enantioseparation scheme.

ASSOCIATED CONTENT

Supporting Information

The Supporting Information is available free of charge at https://pubs.acs.org/doi/10.1021/acs.jpcc.3c00502.

Further information regarding the computational methods, simulations of the HSOH molecule, and additional simulations of propylene oxide frictional enantioseparation (PDF)

AUTHOR INFORMATION

Corresponding Author

Oded Hod − *School of Chemistry and The Sackler Center for Computational Molecular and Materials Science, Tel Aviv University, Tel Aviv 6997801, Israel;* orcid.org/0000-0003-3790-8613; Email: odedhod@tauex.tau.ac.il

Authors

Yun Chen − *School of Chemistry and The Sackler Center for Computational Molecular and Materials Science, Tel Aviv University, Tel Aviv 6997801, Israel*

Long Xu − *AMOS and Department of Chemical and Biological Physics, The Weizmann Institute of Science, Rehovot 7610001, Israel;* orcid.org/0000-0001-5314-2799

Michael Urbakh − *School of Chemistry and The Sackler Center for Computational Molecular and Materials Science, Tel Aviv University, Tel Aviv 6997801, Israel;* orcid.org/0000-0002-3959-5414

Complete contact information is available at: https://pubs.acs.org/10.1021/acs.jpcc.3c00502

Notes

The authors declare no competing financial interest.

https://doi.org/10.1021/acs.jpcc.3c00502
J. Phys. Chem. C 2023, 127, 10997−11004

■ ACKNOWLEDGMENTS

The authors thank Prof. Ilya Averbukh and Prof. Sharly Fleischer for fruitful discussions. O.H. is grateful for generous financial support of the Israel Science Foundation under grant no. 1586/17, the Heineman Chair in Physical Chemistry, and the Naomi Foundation for generous financial support via the 2017 Kadar Award. M.U. acknowledges financial support of the Israel Science Foundation, grant no. 1141/18. M.U. and O.H. acknowledge partial computational support from the Tel Aviv University Center for Nanoscience and Nanotechnology.

■ REFERENCES

(1) Gal, J. Pasteur and the Art of Chirality. *Nat. Chem.* **2017**, *9*, 604−605.
(2) Bonner, W. A. Chirality and Life. *Origins Life Evol. Biosphere* **1995**, *25*, 175−190.
(3) Kravets, N.; Aleksanyan, A.; Chraïbi, H.; Leng, J.; Brasselet, E. Optical Enantioseparation of Racemic Emulsions of Chiral Microparticles. *Phys. Rev. Appl.* **2019**, *11*, No. 044025.
(4) Agranat, I.; Caner, H.; Caldwell, J. Putting Chirality to Work: The Strategy of Chiral Switches. *Nat. Rev. Drug Discovery* **2002**, *1*, 753−768.
(5) Yoon, T. P.; Jacobsen, E. N. Privileged Chiral Catalysts. *Science* **2003**, *299*, 1691−1693.
(6) Higuchi, A.; Tamai, M.; Ko, Y.-A.; Tagawa, Y.-I.; Wu, Y.-H.; Freeman, B. D.; Bing, J.-T.; Chang, Y.; Ling, Q.-D. Polymeric Membranes for Chiral Separation of Pharmaceuticals and Chemicals. *Polym. Rev.* **2010**, *50*, 113−143.
(7) Blaser, H.-U. Chirality and Its Implications for the Pharmaceutical Industry. *Rend. Lincei* **2013**, *24*, 213−216.
(8) Ribeiro, A. R.; Maia, A. S.; Cass, Q. B.; Tiritan, M. E. Enantioseparation of Chiral Pharmaceuticals in Biomedical and Environmental Analyses by Liquid Chromatography: An Overview. *J. Chromatogr., B* **2014**, *968*, 8−21.
(9) Basheer, A. A. Chemical Chiral Pollution: Impact on the Society and Science and Need of the Regulations in the 21 St Century. *Chirality* **2018**, *30*, 402−406.
(10) Gogoi, A.; Mazumder, N.; Konwer, S.; Ranawat, H.; Chen, N.-T.; Zhuo, G.-Y. Enantiomeric Recognition and Separation by Chiral Nanoparticles. *Molecules* **2019**, *24*, 1007.
(11) Marichez, V.; Tassoni, A.; Cameron, R. P.; Barnett, S. M.; Eichhorn, R.; Genet, C.; Hermans, T. M. Mechanical Chiral Resolution. *Soft Matter* **2019**, *15*, 4593−4608.
(12) Carrão, D. B.; Perovani, I. S.; de Albuquerque, N. C. P.; de Oliveira, A. R. M. Enantioseparation of Pesticides: A Critical Review. *TrAC, Trends Anal. Chem.* **2020**, *122*, No. 115719.
(13) Okamoto, Y.; Ikai, T. Chiral HPLC for Efficient Resolution of Enantiomers. *Chem. Soc. Rev.* **2008**, *37*, 2593−2608.
(14) Ward, T. J.; Ward, K. D. Chiral Separations: A Review of Current Topics and Trends. *Anal. Chem.* **2012**, *84*, 626−635.
(15) Fernandes, C.; Tiritan, M.; Pinto, M. Chiral Separation in Preparative Scale: A Brief Overview of Membranes as Tools for Enantiomeric Separation. *Symmetry* **2017**, *9*, 206.
(16) Huang, X.-Y.; Pei, D.; Liu, J.-F.; Di, D.-L. A Review on Chiral Separation by Counter-Current Chromatography: Development, Applications and Future Outlook. *J. Chromatogr. A* **2018**, *1531*, 1−12.
(17) Sun, B.; Kim, Y.; Wang, Y.; Wang, H.; Kim, J.; Liu, X.; Lee, M. Homochiral Porous Nanosheets for Enantiomer Sieving. *Nat. Mater.* **2018**, *17*, 599−604.
(18) Chang, C.; Wang, X.; Bai, Y.; Liu, H. Applications of Nanomaterials in Enantioseparation and Related Techniques. *TrAC, Trends Anal. Chem.* **2012**, *39*, 195−206.
(19) Banerjee-Ghosh, K.; Ben Dor, O.; Tassinari, F.; Capua, E.; Yochelis, S.; Capua, A.; Yang, S. H.; Parkin, S. S. P.; Sarkar, S.; Kronik, L.; Baczewski, L. T.; Naaman, R.; Paltiel, Y. Separation of Enantiomers by Their Enantiospecific Interaction with Achiral Magnetic Substrates. *Science* **2018**, *360*, 1331−1334.
(20) Eilam, A.; Shapiro, M. Spatial Separation of Dimers of Chiral Molecules. *Phys. Rev. Lett.* **2013**, *110*, No. 213004.
(21) Wang, S. B.; Chan, C. T. Lateral Optical Force on Chiral Particles near a Surface. *Nat. Commun.* **2014**, *5*, 3307.
(22) Zhao, Y.; Saleh, A. A. E.; Dionne, J. A. Enantioselective Optical Trapping of Chiral Nanoparticles with Plasmonic Tweezers. *ACS Photonics* **2016**, *3*, 304−309.
(23) Pérez, C.; Steber, A. L.; Domingos, S. R.; Krin, A.; Schmitz, D.; Schnell, M. Coherent Enantiomer-Selective Population Enrichment Using Tailored Microwave Fields. *Angew. Chem., Int. Ed.* **2017**, *56*, 12512−12517.
(24) Vitanov, N. V.; Drewsen, M. Highly Efficient Detection and Separation of Chiral Molecules through Shortcuts to Adiabaticity. *Phys. Rev. Lett.* **2019**, *122*, No. 173202.
(25) Solomon, M. L.; Hu, J.; Lawrence, M.; García-Etxarri, A.; Dionne, J. A. Enantiospecific Optical Enhancement of Chiral Sensing and Separation with Dielectric Metasurfaces. *ACS Photonics* **2019**, *6*, 43−49.
(26) Yachmenev, A.; Onvlee, J.; Zak, E.; Owens, A.; Küpper, J. Field-Induced Diastereomers for Chiral Separation. *Phys. Rev. Lett.* **2019**, *123*, No. 243202.
(27) Leibscher, M.; Giesen, T. F.; Koch, C. P. Principles of Enantio-Selective Excitation in Three-Wave Mixing Spectroscopy of Chiral Molecules. *J. Chem. Phys.* **2019**, *151*, No. 014302.
(28) Solomon, M. L.; Saleh, A. A. E.; Poulikakos, L. V.; Abendroth, J. M.; Tadesse, L. F.; Dionne, J. A. Nanophotonic Platforms for Chiral Sensing and Separation. *Acc. Chem. Res.* **2020**, *53*, 588−598.
(29) Fang, L.; Wang, J. Optical Trapping Separation of Chiral Nanoparticles by Subwavelength Slot Waveguides. *Phys. Rev. Lett.* **2021**, *127*, No. 233902.
(30) Stapelfeldt, H.; Seideman, T. Colloquium: Aligning Molecules with Strong Laser Pulses. *Rev. Mod. Phys.* **2003**, *75*, 543−557.
(31) Yachmenev, A.; Yurchenko, S. N. Detecting Chirality in Molecules by Linearly Polarized Laser Fields. *Phys. Rev. Lett.* **2016**, *117*, No. 033001.
(32) Gershnabel, E.; Averbukh, I. S. Orienting Asymmetric Molecules by Laser Fields with Twisted Polarization. *Phys. Rev. Lett.* **2018**, *120*, 1−6.
(33) Tutunnikov, I.; Gershnabel, E.; Gold, S.; Averbukh, I. S. Selective Orientation of Chiral Molecules by Laser Fields with Twisted Polarization. *J. Phys. Chem. Lett.* **2018**, *9*, 1105−1111.
(34) Tutunnikov, I.; Floß, J.; Gershnabel, E.; Brumer, P.; Averbukh, I. S. Laser-Induced Persistent Orientation of Chiral Molecules. *Phys. Rev. A* **2019**, *100*, No. 043406.
(35) Milner, A. A.; Fordyce, J. A. M.; Macphail-Bartley, I.; Wasserman, W.; Milner, V.; Tutunnikov, I.; Averbukh, I. S. Controlled Enantioselective Orientation of Chiral Molecules with an Optical Centrifuge. *Phys. Rev. Lett.* **2019**, *122*, No. 223201.
(36) Koch, C. P.; Lemeshko, M.; Sugny, D. Quantum Control of Molecular Rotation. *Rev. Mod. Phys.* **2019**, *91*, No. 035005.
(37) Xu, L.; Tutunnikov, I.; Gershnabel, E.; Prior, Y.; Averbukh, I. S. Long-Lasting Molecular Orientation Induced by a Single Terahertz Pulse. *Phys. Rev. Lett.* **2020**, *125*, No. 013201.
(38) Tutunnikov, I.; Floß, J.; Gershnabel, E.; Brumer, P.; Averbukh, I. S.; Milner, A. A.; Milner, V. Observation of Persistent Orientation of Chiral Molecules by a Laser Field with Twisted Polarization. *Phys. Rev. A* **2020**, *101*, No. 021403.
(39) Tutunnikov, I.; Xu, L.; Field, R. W.; Nelson, K. A.; Prior, Y.; Averbukh, I. S. Enantioselective Orientation of Chiral Molecules Induced by Terahertz Pulses with Twisted Polarization. *Phys. Rev. Res.* **2021**, *3*, No. 013249.
(40) Xu, L.; Tutunnikov, I.; Prior, Y.; Averbukh, I. S. Three Dimensional Orientation of Small Polyatomic Molecules Excited by Two-Color Femtosecond Pulses. *J. Phys. B: At., Mol. Opt. Phys.* **2021**, *54*, 164003.
(41) Xu, L. Enantioselective Chiral Orientation Induced by a Combination of a Long and a Short Laser Pulse. *Phys. Rev. A* **2022**, *105*, No. 033113.

https://doi.org/10.1021/acs.jpcc.3c00502
J. Phys. Chem. C 2023, 127, 10997−11004

(42) Xu, L.; Tutunnikov, I.; Prior, Y.; Averbukh, I. S. Optimization of the Double-Laser-Pulse Scheme for Enantioselective Orientation of Chiral Molecules. *J. Chem. Phys.* **2022**, *157*, No. 034304.
(43) Loesch, H. J.; Remscheid, A. Brute Force in Molecular Reaction Dynamics: A Novel Technique for Measuring Steric Effects. *J. Chem. Phys.* **1990**, *93*, 4779−4790.
(44) Friedrich, B.; Herschbach, D. R. Spatial Orientation of Molecules in Strong Electric Fields and Evidence for Pendular States. *Nature* **1991**, *353*, 412−414.
(45) Bulthuis, J.; Möller, J.; Loesch, H. J. Brute Force Orientation of Asymmetric Top Molecules. *J. Phys. Chem. A* **1997**, *101*, 7684−7690.
(46) Kuipers, E. W.; Tenner, M. G.; Kleyn, A. W.; Stolte, S. Observation of Steric Effects in Gas−Surface Scattering. *Nature* **1988**, *334*, 420−422.
(47) Tenner, M. G.; Kuipers, E. W.; Kleyn, A. W.; Stolte, S. Direct Inelastic Scattering of Oriented NO from Ag(111) and Pt(111). *J. Chem. Phys.* **1991**, *94*, 5197−5207.
(48) Greeley, J. N.; Martin, J. S.; Morris, J. R.; Jacobs, D. C. Scattering Aligned NO^+ on Ag(111): The Effect of Internuclear-Axis Direction on NO^- and O^- Product Formation. *J. Chem. Phys.* **1995**, *102*, 4996−5011.
(49) Henriksen, N. E. Laser Control of Chemical Reactions. *Chem. Soc. Rev.* **2002**, *31*, 37−42.
(50) Shreenivas, D.; Lee, A.; Walter, N.; Sampayo, D.; Bennett, S.; Seideman, T. Intense Laser Alignment as a Route to Control of Surface Reactions. *J. Phys. Chem. A* **2010**, *114*, 5674−5681.
(51) Khodorkovsky, Y.; Manson, J. R.; Averbukh, I. S. Modifying Molecule-Surface Scattering by Ultrashort Laser Pulses. *Phys. Rev. A* **2011**, *84*, No. 053420.
(52) Khodorkovsky, Y.; Manson, J. R.; Averbukh, I. S. Modifying Molecular Scattering from Rough Solid Surfaces Using Ultrashort Laser Pulses. *Mol. Phys.* **2013**, *111*, 1716−1730.
(53) Vovk, I. A.; Baimuratov, A. S.; Zhu, W.; Shalkovskiy, A. G.; Baranov, A. V.; Fedorov, A. V.; Rukhlenko, I. D. Chiral Nanoparticles in Singular Light Fields. *Sci. Rep.* **2017**, *7*, 45925.
(54) Schamel, D.; Pfeifer, M.; Gibbs, J. G.; Miksch, B.; Mark, A. G.; Fischer, P. Chiral Colloidal Molecules and Observation of the Propeller Effect. *J. Am. Chem. Soc.* **2013**, *135*, 12353−12359.
(55) Clemens, J. B.; Kibar, O.; Chachisvilis, M. A Molecular Propeller Effect for Chiral Separation and Analysis. *Nat. Commun.* **2015**, *6*, 7868.
(56) De Gennes, P. G. Mechanical Selection of Chiral Crystals. *Europhys. Lett.* **1999**, *46*, 827−830.
(57) Stroock, A. D.; Dertinger, S. K. W.; Ajdari, A.; Mezić, I.; Stone, H. A.; Whitesides, G. M. Chaotic Mixer for Microchannels. *Science* **2002**, *295*, 647−651.
(58) Kostur, M.; Schindler, M.; Talkner, P.; Hänggi, P. Chiral Separation in Microflows. *Phys. Rev. Lett.* **2006**, *96*, No. 014502.
(59) Marcos; Fu, H. C.; Powers, T. R.; Stocker, R. Separation of Microscale Chiral Objects by Shear Flow. *Phys. Rev. Lett.* **2009**, *102*, No. 158103.
(60) Eichhorn, R. Microfluidic Sorting of Stereoisomers. *Phys. Rev. Lett.* **2010**, *105*, No. 034502.
(61) Meinhardt, S.; Smiatek, J.; Eichhorn, R.; Schmid, F. Separation of Chiral Particles in Micro- or Nanofluidic Channels. *Phys. Rev. Lett.* **2012**, *108*, No. 214504.
(62) Aristov, M.; Eichhorn, R.; Bechinger, C. Separation of Chiral Colloidal Particles in a Helical Flow Field. *Soft Matter* **2013**, *9*, 2525−2530.
(63) Beleke-Maxwell, K.; Franke, T.; Hoppe, R. H. W.; Linsenmann, C. Numerical Simulation of Surface Acoustic Wave Actuated Enantiomer Separation by the Finite Element Immersed Boundary Method. *Comput. Fluids* **2015**, *112*, 50−60.
(64) Burger, S.; Franke, T.; Fraunholz, T.; Hoppe, R. H. W.; Peter, M. A.; Wixforth, A. Numerical Simulation of Surface Acoustic Wave Actuated Separation of Rigid Enantiomers by the Fictitious Domain Lagrange Multiplier Method. *Comput. Methods Appl. Math.* **2015**, *15*, 247−258.
(65) Aquilanti, V.; Maciel, G. S. Observed Molecular Alignment in Gaseous Streams and Possible Chiral Effects in Vortices and in Surface Scattering. *Origins Life Evol. Biosphere* **2007**, *36*, 435−441.
(66) Lee, H. N.; Chang, L. C.; Su, T. M. Optical Rotamers of Substituted Simple Alkanes Induced by Macroscopic Translation-Rotational Motions. *Chem. Phys. Lett.* **2011**, *507*, 63−68.
(67) Lee, H.-N.; Chao, I.; Su, T.-M. Asymmetry in the Internal Energies of the Optical Rotamers of 1-Bromo-2-Chloroethane in Oriented-Molecule/Surface Scattering: A Classical Molecular Dynamics Study. *Chem. Phys. Lett.* **2011**, *517*, 132−138.
(68) Lombardi, A.; Palazzetti, F. Chirality in Molecular Collision Dynamics. *J. Phys.: Condens. Matter* **2018**, *30*, No. 063003.
(69) Winnewisser, G.; Lewen, F.; Thorwirth, S.; Behnke, M.; Hahn, J.; Gauss, J.; Herbst, E. Gas-Phase Detection of HSOH: Synthesis by Flash Vacuum Pyrolysis of Di-Tert-Butyl Sulfoxide and Rotational-Torsional Spectrum. *Chem. - Eur. J.* **2003**, *9*, 5501−5510.
(70) Yurchenko, S. N.; Yachmenev, A.; Thiel, W.; Baum, O.; Giesen, T. F.; Melnikov, V. V.; Jensen, P. An Ab Initio Calculation of the Vibrational Energies and Transition Moments of HSOH. *J. Mol. Spectrosc.* **2009**, *257*, 57−65.
(71) Plimpton, S. Fast Parallel Algorithms for Short-Range Molecular Dynamics. *J. Comput. Phys.* **1995**, *117*, 1−19.
(72) Jorgensen, W. L.; Maxwell, D. S.; Tirado-Rives, J. Development and Testing of the OPLS All-Atom Force Field on Conformational Energetics and Properties of Organic Liquids. *J. Am. Chem. Soc.* **1996**, *118*, 11225−11236.
(73) Yanai, T.; Tew, D. P.; Handy, N. C. A New Hybrid Exchange−Correlation Functional Using the Coulomb-Attenuating Method (CAM-B3LYP). *Chem. Phys. Lett.* **2004**, *393*, 51−57.
(74) Frisch, M. J.; Trucks, G. W.; Schlegel, H. B.; Scuseria, G. E.; Robb, M. A.; Cheeseman, J. R.; Scalmani, G.; Barone, V.; Petersson, G. A.; Nakatsuji, H.; et al. *Gaussian 16*; Gaussian, Inc.: Wallingford, CT, 2016.
(75) Israelachvili, J. N. *Intermolecular and Surface Forces*; Academic Press, 2011.
(76) Mehta, N. A.; Murray, V. J.; Xu, C.; Levin, D. A.; Minton, T. K. Nonreactive Scattering of N_2 from Layered Graphene Using Molecular Beam Experiments and Molecular Dynamics. *J. Phys. Chem. C* **2018**, *122*, 9859−9874.
(77) Majumder, M.; Gibson, K. D.; Sibener, S. J.; Hase, W. L. Chemical Dynamics Simulations and Scattering Experiments for O_2 Collisions with Graphite. *J. Phys. Chem. C* **2018**, *122*, 16048−16059.
(78) Kurahashi, M.; Kondo, T. Alignment-Resolved O_2 Scattering from Highly Oriented Pyrolytic Graphite and LiF(001) Surfaces. *Phys. Rev. B* **2019**, *99*, No. 045439.
(79) Greenwood, T.; Koehler, S. P. K. Nitric Oxide Scattering off Graphene Using Surface-Velocity Map Imaging. *J. Phys. Chem. C* **2021**, *125*, 17853−17860.
(80) Hummer, G.; Rasaiah, J. C.; Noworyta, J. P. Water Conduction through the Hydrophobic Channel of a Carbon Nanotube. *Nature* **2001**, *414*, 188−190.
(81) Weisstein, E. W. *"Gaussian Function" MathWorld-A Wolfram Web Resource*; http://mathworld.wolfram.com/GaussianFunction.html.
(82) Sussman, B. J. Five Ways to the Nonresonant Dynamic Stark Effect. *Am. J. Phys.* **2011**, *79*, 477−484.
(83) Kleyn, A. W.; Luntz, A. C.; Auerbach, D. J. Rotational Energy Transfer in Direct Inelastic Surface Scattering: NO on Ag(111). *Phys. Rev. Lett.* **1981**, *47*, 1169−1172.

https://doi.org/10.1021/acs.jpcc.3c00502
J. Phys. Chem. C 2023, 127, 10997−11004